Mechanics of Materials 6 (1987) 71–87
North-Holland



# FINITE ELEMENT METHOD SIMULATION OF CRACK PROPAGATION IN A BRITTLE MICROCRACKING SOLID

P.G. CHARALAMBIDES * and R.M. McMEEKING

*Materials Program, College of Engineering, University of California, Santa Barbara, CA 93106, U.S.A.*

Received 23 July 1986; revised version received 18 December 1986

A finite element method simulation of crack propagation was used to study the effects of microcracking at facets as a damage process in brittle composites and the consequence for material toughness. A continuum model for microcracking at grain boundary facets was used in conjunction with the elasticity law. The model accounts for modulus reduction only and neglects residual strain effects. The nonlinear finite element equations were solved incrementally. The solution for each load increment was obtained using a Newton iteration method. Crack propagation was achieved by successive tip node relaxation upon satisfaction of a critical energy release rate criterion. The crack was allowed to propagate by approximately ten times the height of the initial microcrack zone. A substantial increase of the height of the damage zone prior to steady state propagation was observed. The applied stress intensity factor was increased to sustain crack growth, and crack tip shielding occurs as a result of the wake. The amount of toughening was up to 40% in terms of stress intensity factor and was influenced by the parameters of the constitutive law. Stress, strain, and microcrack density distributions near the tip of the steadily growing crack are discussed.

## 1. Introduction

Microcracking after processing is sometimes observed in ceramics (Evans and Langdon, 1976; Evans, Heuer and Porter, 1977). Typically ceramics are processed at high temperatures and cooled to ambient. This causes thermal stresses dominated by expansion mismatches in multi-phase ceramics and thermal expansion anisotropies in single phase systems. Single phase ceramics microcrack along the grain boundaries (Fu, 1983; Evans and Fu, 1985a; 1985b) whereas two phase ceramics microcrack at the particle/matrix interface (Evans and Faber, 1981; 1984). Generally, the resistance to microcracking is grain and particle size dependent with larger grain and particle sizes allowing microfracture more readily (Evans and Fu, 1985b; Evans and Faber, 1981; Evans, 1974). If microstructure sizes are sufficiently large, spontaneous microcracking can occur on cooling after processing. However, grain or particle size can be controlled during processing so that this damage can be avoided. The residual stresses remain after processing, however, and if a sufficiently high external stress is applied to the material, microcracking can occur as a result of the combination of external and internal stress. This situation can be caused by the intensificiation of stress at the tip of a large crack. Consequently a microcrack zone, analogous to a plastic zone, develops at such crack tips (Hoagland et al. 1974; Friedman, Handin and Alani, 1972). This zone can have at least two effects on the propagation of the large crack. The damaged material provides a weak path for the crack and so causes crack growth more readily. On the other hand, the microcracks can shield the major crack from stress and provide a toughening mechanism. Indeed, toughness enhancement in conjunction with microcracking is observed in practice (Hubner and Jillek, 1977; Knehans and Steinbrech, 1982). In our paper, we consider the mechanics of near tip microcracking and report on calculations for macroscopic crack growth in such microcracking materials.

* Graduate student at the Department of Theoretical and Applied Mechanics, University of Illinois at Urbana-Champaign.

Following Fu (1983) and Evans and Fu (1985b) we shall consider facet microcracking in single phase ceramics as illustrated schematically in Fig. 1. Some grain boundaries may crack spontaneously on cooling, but we shall assume that the grain size is small enough so that the number involved is negligible. When tensile stress is applied to the ceramic, favorably oriented facets subject to large residual tensile stress will crack. The failure is stable because neighboring grain boundaries are less favorably oriented and probably subject to lower tensile stresses. As the stress is raised, more facets crack and so damage is progressive with applied stress. Consider a macroscopic element of the material. As the number of microcracks in the element increases, the material will become more compliant. Anisotropy will develop since the maximum principal tensile stress will influence microcrack orientations. Finally, as residual tensile stresses on facets are relieved by cracking, an increment of strain will occur at fixed stress (Evans and Faber, 1981; 1984).

We will make use of the developments of Fu (1983) and Evans and Fu (1985b) and use a continuum model to describe this material. Our model is slightly different from that in Fu (1983) but retains all the major features. As in their work, the anisotropy is neglected as a less significant contribution than modulus reduction. The modulus reduction is introduced, as in Fu (1983) and Evans and Fu (1985a, 1985b), by the self-consistent formulation of Budiansky and O'Connell (1975). That formulation accounts for long range interactions among the microcracks but neglects the nearest neighbor effects. As such, it introduces interactions at a level similar to that in the works of Chudnovsky and Kachanov (1983) and Rose (1986a). However, the Budiansky and O'Connell model allows us to account at the outset for finite microcracks (of penny shape) which are randomly distributed in the material matrix. Anisotropy arises in general because failure mechanisms favor the generation of microcracks oriented normal to the applied stress. The effect of this on the elastic response of the material could be accounted for using the work of Hoenig (1979) on such anisotropic microcrack distributions. However, the anisotropy is thought to be not very great because it is largely the residual stresses that contribute to the microcracking process, with the applied stress providing a relatively small increment up to the criticial condition. The residual stresses are random as to orientation and so the microcracking will be almost random with a slight bias due to the applied stress. In consequence of this, a purely isotropic reduced modulus approach has been adopted.

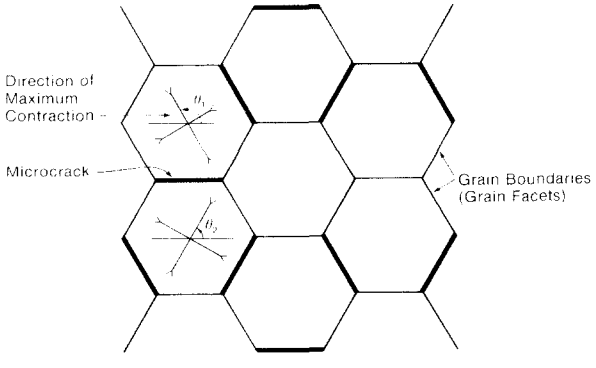


Fig. 1. A random set of facet microcracks in a typical hexogonal grain network.

Another possible source of anisotropy is selective closure of microcracks due to compressive stresses. Models for this phenomenon have been developed by Horii and Nemat-Nasser (1983b; 1985). The effect is likely to occur in ceramics like alumina, especially in the wake region created by a growing microcrack. However, this anisotropy will be limited by the fact that the residual stresses which cause the microfractures will also cause the resulting flaws to remain open even when there is zero applied stress. As a result, there has to be substantial compression before the microcracks close. In addition, the microcracks are created in the crack tip region where all of the principal stresses are tensile and the question of closure does not arise there. In view of the weak anisotropic effect associated with closure in the wake region behind the crack tip, the effect has been neglected.

As noted above, the residual stresses relieved by microcracking cause the flaws to be open even when there is no applied stress acting on the material element. As a result of this, there will be a residual strain in macroscopic samples of the

microcracked material when free of applied stress. That is, material loaded to cause microcracking and then unloaded will have a residual dilatation. This will make a significant contribution to the toughening effect of microcracks (Evans and Faber, 1981; 1984; Fu, 1983; Evans and Fu, 1985b). The effect has been incorporated into numerical calculations by Charalambides (1986) and Charalambides and McMeeking (1986b). The purpose of this paper is to address the modulus reduction effect on toughening by itself, and the work just referred to should be considered a sequel to this paper, with residual strain effects included. However, the effect of residual stresses as far as retention of the predominant isotropy of the material response is concerned is considered to prevail even though the residual strain resulting from it are neglected in this paper. Thus the macroscopic stress–strain response of the material is as shown in Fig. 2 with nonlinear behavior caused by microcracking followed by a return to zero strain upon unloading.

The continuum constitutive law that results is used in calculations of the development of microcrack zones around a plane strain macroscopic crack tip. Previous calculations (Charalambides and McMeeking, 1986a) have indicated that microcracking has little or no effect on crack growth initiation. These calculations were carried out for stationary cracks. It must be deduced that as the crack grows, resistance to crack growth builds up by the formation of a wake of microcracked material. This wake contributed to the shielding of the crack tip and so a resistance or R-curve (Knehans and Steinbrech, 1982; McMeeking and Evans, 1982) is a feature of the fracture behavior of this material. That is, the crack tip stress intensity factor as measured from the applied load increases as the crack grows. As in plane stress behavior in metals, the R-curve influences the stability of the crack growth and thus determines the level of effective fracture toughness that can be achieved.

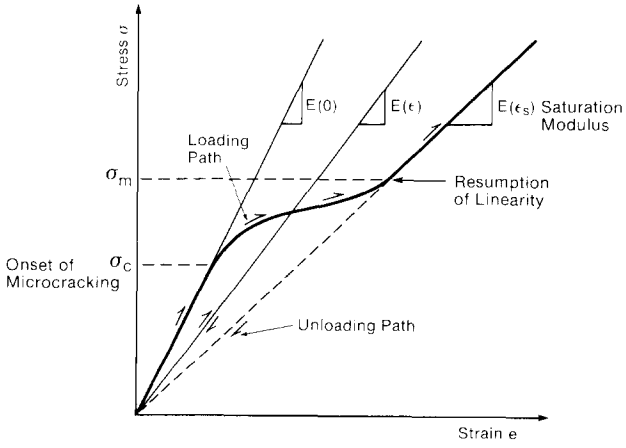


Fig. 2. The stress–strain relation for a microcracking material with no residual strains.

The objective of this work is to quantify the mechanics of microcrack toughening by simulation of crack propagation in finite element calculations using the continuum constitutive law for a microcracking material. Small scale microcrack zones are ensured by the level of applied loading and crack growth commences when a critical energy release rate at the crack tip is achieved. As discussed by Charalambides and McMeeking (1986a), the constitutive law is such that the microcrack density is allowed to saturate to a finite level at high stress. As a consequence, the material adjacent to the crack tip is linear elastic although with a reduced modulus. It follows that the concepts of stress intensity factor and energy release rate are valid for the crack tip. The crack growth is simulated by nodal release when the critical crack tip energy release rate for propagation is exceeded. Growth continues until the criterion fails. Then, the applied loads are increased until the critical condition for growth is exceeded again, at which stage another node is released to cause a step of crack propagation. This process is continued until the length of the crack growth is several times the microcrack zone size. The energy release rate and stress intensity factor as computed from the applied loads can be obtained and plotted against the amount of crack growth. These R-curves can be used to provide information about the magnitude of microcrack toughening. In addition, the steady state toughening results obtained from this work will be compared with the less exact results of Charalambides and McMeeking (1986a) which were obtained by interpretation of stationary crack results.

## The continuum microcracking solid

The self-consistent microcracking model developed by Fu (1983) and Evans and Fu (1985a) and used in earlier work on microcracking solids by Charalambides and McMeeking (1986a) will be used throughout the present analysis to describe the behavior of the stress-induced microcracking material. The microcracking law relating stress magnitudes to microcrack density values is given as follows. For monotonically increasing loading, if

$$\begin{aligned}
&\sigma_e < \sigma_c && \text{then } \epsilon = 0, \\
&\text{material remains unmicrocracked;} \\
&\sigma_c \leqslant \sigma_e \leqslant \sigma_m && \text{then } \epsilon = \lambda(\sigma_e - \sigma_c), \\
&\text{the microcrack density is increasing} \\
&\quad \text{linearly with } \boldsymbol{\sigma}; \\
&\sigma_e > \sigma_m && \text{then } \epsilon = \lambda(\sigma_m - \sigma_c) = \epsilon_s, \\
&\text{the microcrack density is saturated.}
\end{aligned} \tag{1}$$

The term $\epsilon$ is the microcrack density, $\sigma_e = \sqrt{\sigma_{ij}\sigma_{ij}}$ is an equivalent stress measure, $\boldsymbol{\sigma}$ is the macroscopic stress tensor, $\sigma_c$ is the critical stress for microcracking initiation, $\sigma_m$ determines saturation microcrack density value $\epsilon_s$ and $\lambda$ is the microcracking rate with stress. The scalar measure of stress, $\sigma_e$, has been chosen to control microcracking because it conforms to some extent with the findings of Evans and Fu (1985a) in that regard. In addition, use of $\sigma_e$ leads below to a hyperelastic constitutive law for cases in which $\sigma_e$ increases monotonically. This in turn leads to a path independent $J$-integral (Rice, 1986) for stationary crack problems.

The microcrack density $\epsilon$ is as defined by Budiansky and O'Connell (1975) and is proportional to the number of microcracks per unit volume times an effective volume for the microcracks. When there are $N$ circular microcracks per unit volume on grain boundary facets and each microcrack has a radius $\frac{1}{2}l$ then $\epsilon = \frac{1}{8}Nl^3$, where $l$ is the facet length. We also note that $\epsilon$ cannot decrease. As will be seen later, the parameters of the microcracking law can be tied to microstructural features. The expressions for the effective elastic properties of a microcracked solid obtained by Budiansky and O'Connell (1975) were approximated by Charalambides and McMeeking (1986a) as follows

$$\frac{\bar{E}}{E} = \frac{\bar{\nu}}{\nu} = 1 - \tfrac{16}{9}\epsilon = \frac{1}{f} \tag{2}$$

where $\bar{E}$, $E$ and $\bar{\nu}$, $\nu$ are the Young's Modulus and Poisson's ratios of the microcracked and unmicrocracked solid respectively. The parameter $f$ is a microcracking internal variable, and from equation (1) it can be seen that it is a function of stress and stress history. Then the constitutive law of the microcracking solid is as follows

$$\epsilon_{ij} = \frac{f+\nu}{E}\sigma_{ij} - \frac{\nu}{E}\sigma_{kk}\delta_{ij} \tag{3}$$

where $\sigma_{ij}$ is the macroscopic stress tensor, $\epsilon_{ij}$ the macroscopic strains, and $\delta_{ij}$ the Kronecker delta. It is useful to state the above constitutive relations in the following forms

$$\begin{aligned}
\sigma_{ij} &= C_{ijkl}\epsilon_{kl} \\
&= \frac{E}{f+\nu}\left[\epsilon_{ij} + \frac{\nu}{f-2\nu}\epsilon_{ij}\delta_{ij}\right].
\end{aligned} \tag{4}$$

For plane problems

$$\epsilon_{\alpha\beta} = \frac{f+\nu}{E}\left[\sigma_{\alpha\beta} - \nu^*\sigma_{\gamma\gamma}\delta_{\alpha\beta}\right], \quad \alpha, \beta, \gamma = 1, 2; \tag{5a}$$

$$\sigma_{\alpha\beta} = \frac{E}{f+\nu}\left[\sigma_{\alpha\beta} + \frac{\nu^*}{1-2\nu^*}\epsilon_{\gamma\gamma}\delta_{\alpha\beta}\right], \quad \alpha, \beta, \gamma = 1, 2, \tag{5b}$$

where $\nu^* = \nu/f$ for plane strain and $\nu^* = \nu/(f+\nu)$ for plane stress. A typical uniaxial stress–strain curve is shown in Fig. 2.

## The boundary value problem

The boundary value problem for the propagating crack is similar to that for the stationary crack case solved by Charalambides and McMeeking (1986a). A circular region around the crack tip is analyzed. To enforce small scale microcracking conditions we choose the outer radius of the region around the crack tip to be far enough so that

the elastic stress field there remains virtually unaffected by the induced microcracking. However, the radius is also small enough that the elastic crack tip singular stresses dominate the solution at the perimeter. The boundary conditons around the outer radius are chosen to enforce this. They are the tractions of the elastic crack tip singular field for mode I (tensile opening). The loads are characterized by $K_I$, the stress intensity factor. This arrangement represents the problem of small scale crack tip microcracking. Symmetry conditions are enforced through appropriate boundary conditions and so only a semicircle as shown in Fig. 3 is used in the calculations. The crack is traction free. Governing equations of equilibrium and compatibility are enforced through the principle of virtual work in the absence of body forces,

$$\int_A \sigma_{ij}\delta\epsilon_{ij}\,dA = \int_{S_T} T_i\delta u_i\,dS \tag{6}$$

where $A$ is the plane area being analyzed, $S_T$ is the perimeter where tractions are prescribed, $\boldsymbol{u}$ are the displacements and the symbol $\delta$ indicates a virtual variation of the quantity following it. The variation disappears on $S - S_T$ where the displacements are prescribed.

The solution to this boundary value problem for a stationary crack will involve a crack tip microcrack zone. The inner core of this zone will be saturated with $\epsilon = \epsilon_s$ and the response of the material in this core will be linear elastic with reduced moduli as given by (2). Consequently the crack tip stresses will have an $r^{-1/2}$ singularity at the tip and a stress intensity factor $K_I^{tip}$ will characterize the stresses. The usual Irwin relationship can be used to give the crack tip energy release rate $G^{tip}$.

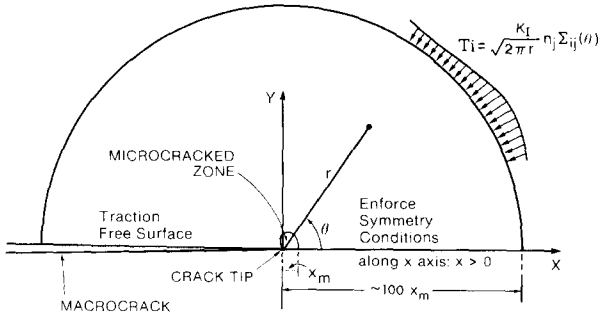


Fig. 3. The boundary conditions used in formulating the microcracking boundary value problem around the crack tip of a major crack under mode I loading.

The constitutive law in (14) is hyperelastic for monotonically increasing $\sigma_e$ and so the $J$-integral (Rice, 1968) is then path independent everywhere in the plane. The hyperelasticity can be demonstrated from the fact that there is a potential $U$ which generates the constitutive law given by (3, 4). This potential has the form

$$U(\sigma) = \frac{1}{E}\int_0^{\sigma_e}(f+\nu)\sigma_e d\sigma_e - \frac{\nu}{2E}(\sigma_{kk})^2 \tag{7}$$

and it should be noted that since $f = f(\sigma_e)$ for monotonic increase of $\sigma_e$, the integral is path independent in stress space as long as $\sigma_e$ increases monotonically. The constitutive law can be generated by the partial derivatives

$$\frac{\partial U}{\partial \sigma_{ij}} = \frac{f+\nu}{E}\sigma_e\frac{\partial \sigma_e}{\partial \sigma_{ij}} - \frac{\nu}{E}\sigma_{kk}\delta_{ij} = \epsilon_{ij}, \tag{8}$$

where the fact that

$$\partial\sigma_e/\partial\sigma_{ij} = \sigma_{ij}/\sigma_e$$

has been used. Since the strain can be obtained from the potential $U$ it follows that a Legendre transformation gives

$$W(\epsilon) = \sigma_{ij}\epsilon_{ij} - U(\sigma) \tag{9}$$

where $W$ is the strain energy density per unit volume and that

$$\sigma_{ij} = \partial W/\partial\epsilon_{ij}. \tag{10}$$

This last result is used in the proof of the path independence of $J$. It should be reiterated that the comments above are only valid for monotonic increases in $\sigma_e$ and thus the path independence of $J$ holds only for stationary cracks during initial loading. From the path independence of $J$ and the fact that $G^{tip} = J$, it follows that for stationary crack subject to monotonically increasing loads

$$G^{tip} = \frac{(1-\nu^2)}{E}K_I^2 = \frac{(1-\bar{\nu}^2)}{\bar{E}}\left(K_I^{tip}\right)^2 \tag{11}$$

where $K_I$ is evaluated in the far field and $\bar{E}$ and $\bar{\nu}$ have their saturated values.

Returning now to the problem formulation, we observe that for the stationary crack, the value of $K_I$ controlling the applied loads is increased until $G^{tip}$ reaches the critical level for crack propagation $G_c^{tip}$. This corresponds to a value of $K_I$ equal to $K_I^c$. The crack begins to grow and is made to continue to grow in such a way that $G^{tip}$ is held fixed at the value $G_c^{tip}$. Equation (11) is no longer valid because of the irreversibility of the constitutive law. To maintain $G^{tip} = G_c^{tip}$, $K_I$ controlling the applied loads must be adjusted during crack growth. As will be seen, $K_I$ always increases during crack growth and the boundary conditions must be altered to maintain the correct singular field relative to the moving crack tip.

## The finite element calculations

The finite element equations can be derived from the principle of virtual work given by equation (6). The above equation and the constitutive law (5) give rise to the nonlinear finite element equations,

$$[K(u_n)]\{u_n\} = \{F_n\} \tag{12}$$

where $[K(u_n)]$ is the stiffness matrix, $\{u_n\}$ is the array of nodal displacements, and the form $[k(u_n)]$ indicates the dependence of the stiffness on the nodal displacements due to the nonlinear constitutive law. The nonlinear finite element equations were solved incrementally. Small increments of load were used to avoid any difficulty with the irreversible constitutive law. Material at integration stations in the finite element mesh was made to remain on the nonlinear loading branch or on the linear unloading branch entirely throughout an increment of load and was not permitted to switch from one branch to another within that step. This means that the material was effectively hyperelastic at the integration stations during a given step, and a Newton iteration scheme was used to obtain satisfactory results for equation (12) at the end of each step. Any switch from loading to unloading took place between steps and was consistently allowed for, according to the constitutive law summarized earlier in this paper. During iterations, a norm of the discrepancy between the actual and computed tractions was used to assess convergence of the solution. It was found that the number of iterations needed to obtain the stationary solution depended on the saturation value of the microcrack density used in the problem. Under very strict convergence requirements, the stationary crack solution was obtained after four iterations for $\epsilon_s = 0.1$ whereas for $\epsilon_s = 0.5$ convergence for the above solution was achieved after ten iterations, indicating the severe effects of high microcrack density values on the non-linearity of the material behavior. When the crack was growing and either a node was being released or an increment of the load was applied, only two or three iterations were needed to update the microcrack density.

The finite element mesh used for the calculations is shown in Fig. 4. The zone of microcracks developed in the inner core mesh shown in Fig. 4(c). The radius of the outer boundary where the tractions were applied was chosen to be approximately 100 times the vertical side of the rectangular inner core mesh shown in Fig. 4(a), thus enforcing small-scale microcracking conditions. In addition, the size of the inner core mesh and therefore the size of the finite elements in that region was chosen so that a sufficiently large number of elements were involved in the saturation microcrack zone for proper calculation of $G^{tip}$. As shown by Charalambides and McMeeking (1986a) for stationary cracks, the saturation zone diminishes significantly as $\epsilon_s$ becomes larger than 0.4. In this case an enormous number of elements would be required for accurate toughening predictions. Such a fine mesh was not possible, and this affected the accuracy of the results, although the trends remained the same and comparison with the less exact results of Charalambides and McMeeking (1986a) can be made. The mesh used contains a total of 1004 four-noded isoparametric elements with four stations for integration of the material stiffness and a total of 1046 nodes. The crack tip was located two elements to the right of the left-hand side of the innermost mesh when the stationary solution was obtained. The crack was caused to propagate when the energy release rate

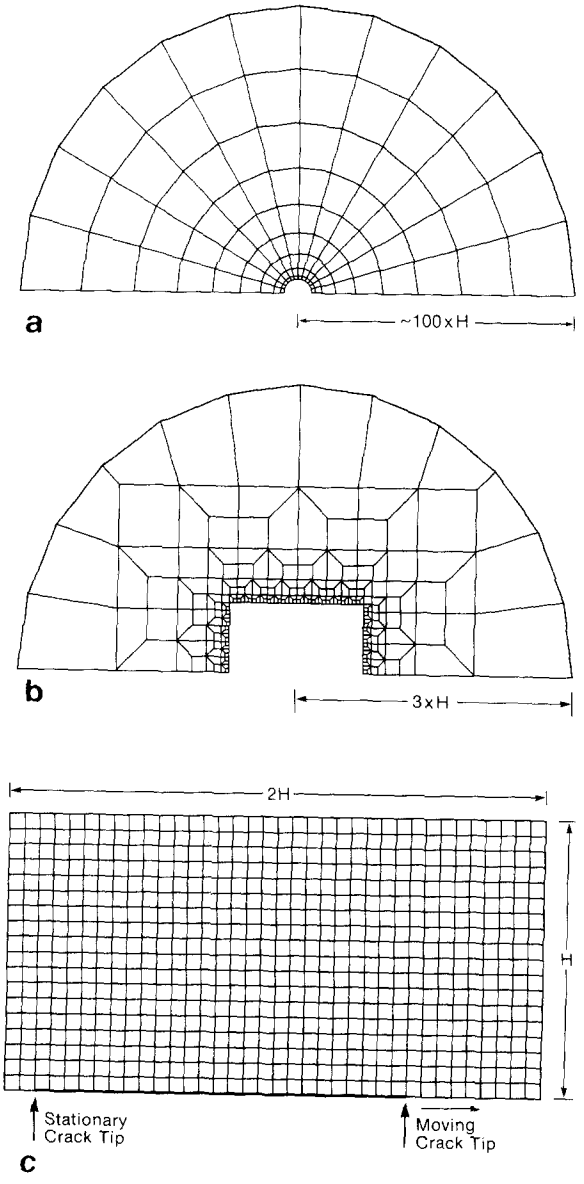


Fig. 4. The finite element mesh used in the finite element crack propagation simulation.

$G^{tip}$ exceeded the critical level. The quantity $G^{tip}$ was computed as needed from a generalized stiffness derivative method of Parks (1974; 1978) modified to allow for the microcracking constitutive law. The strain energy density $W$ used in the above calculations can be found in Appendix I. In our finite element analysis, we modelled the crack propagation by advancing the crack through the finite element mesh using controlled consecutive releases of nodes along the heavy line shown in Fig. 4(c). Once the criterion for initation of crack propagation was exceeded, the node at the crack tip was released, i.e., it was changed from zero normal displacement boundary condition to traction free condition, thus advancing the crack by an element length. The finite element equations were then resolved for the new conditions. Crack propagation steps were repeated until $G^{tip}$ fell below $G_c^{tip}$. At that stage an incremental increase of the applied loads was imposed and a new boundary value problem was solved until the condition for crack propagation was fulfilled again. The procedure was repeated until the crack advanced by a distance approximately equal to ten times the height of the damage zone.

## Results

Figures 5(a) to (f) show the progressive development of the microcracked wake zone as the crack advanced through the finite element mesh. The perimeter of the wake at $\epsilon = 0$ is slightly outside the contour for $\epsilon = 0.01$ shown in the figures. We observe that the width of the process zone increased substantially until steady crack growth conditions were established. This increase was of the order of 100% for saturation microcrack density values $\epsilon_s = 0.5$ as shown in Fig. 6 by the lines marked "maximum zone height", which denote the maximum width of the wake zone measured from the crack surface. The zone height increase was consistent with recent experimental observations of Marshall (1986). In contrast, the height of the completely saturated inner zone increased very little as the crack advanced as shown in Fig. 6 by the other pair of lines. The widening of the microcracked zone became more pronouced as $\epsilon_s \to 0.5$, whereas the corresponding increase for the saturation zone became insignificant.

Figure 7 shows the microcrack density profile in the $y$-direction at different positions in the wake of microcracked material. It is of some interest that the microcrack density varied almost lin-

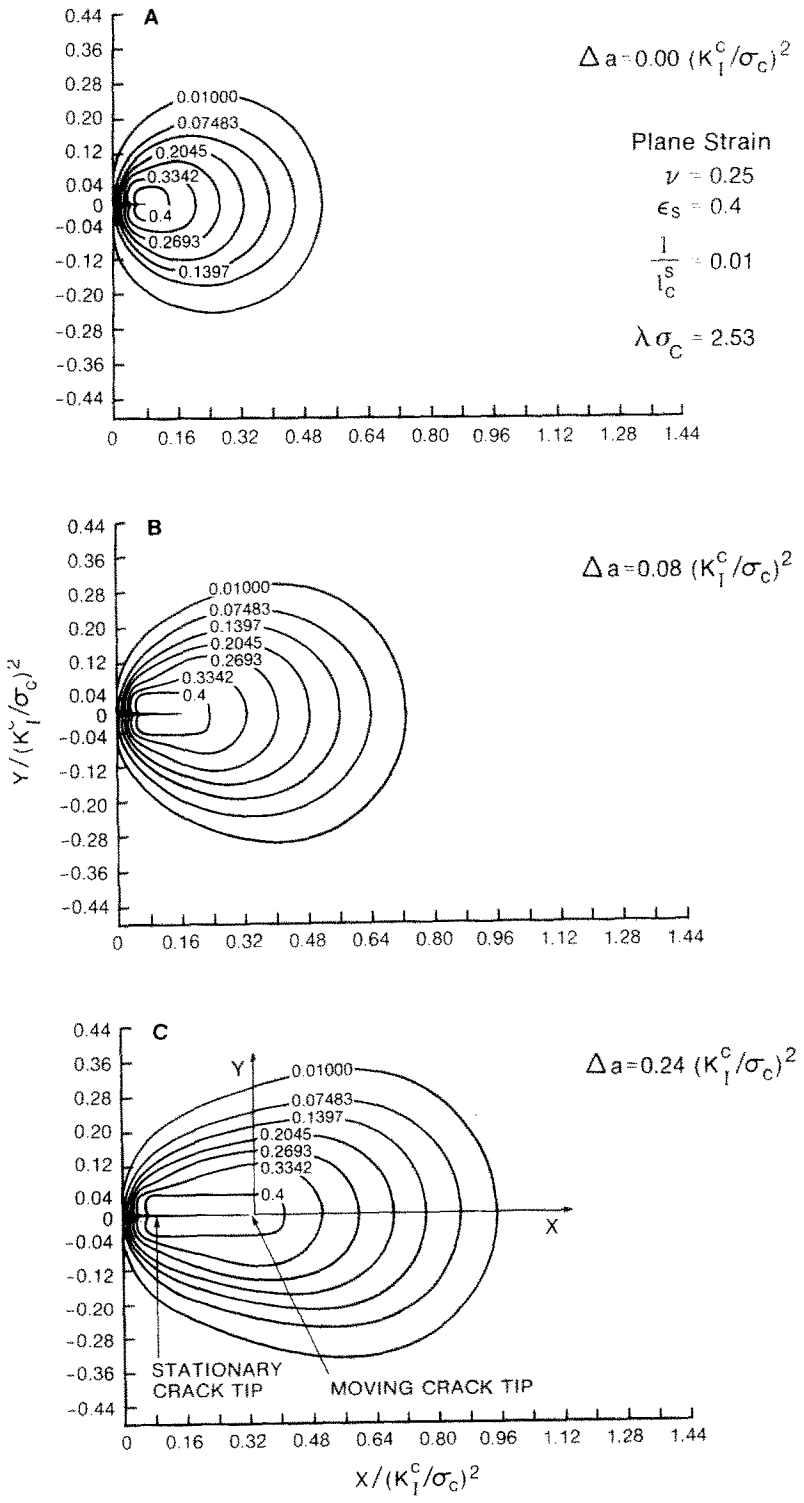


Fig. 5. The microcrack density contours and the wake formation during crack growth.

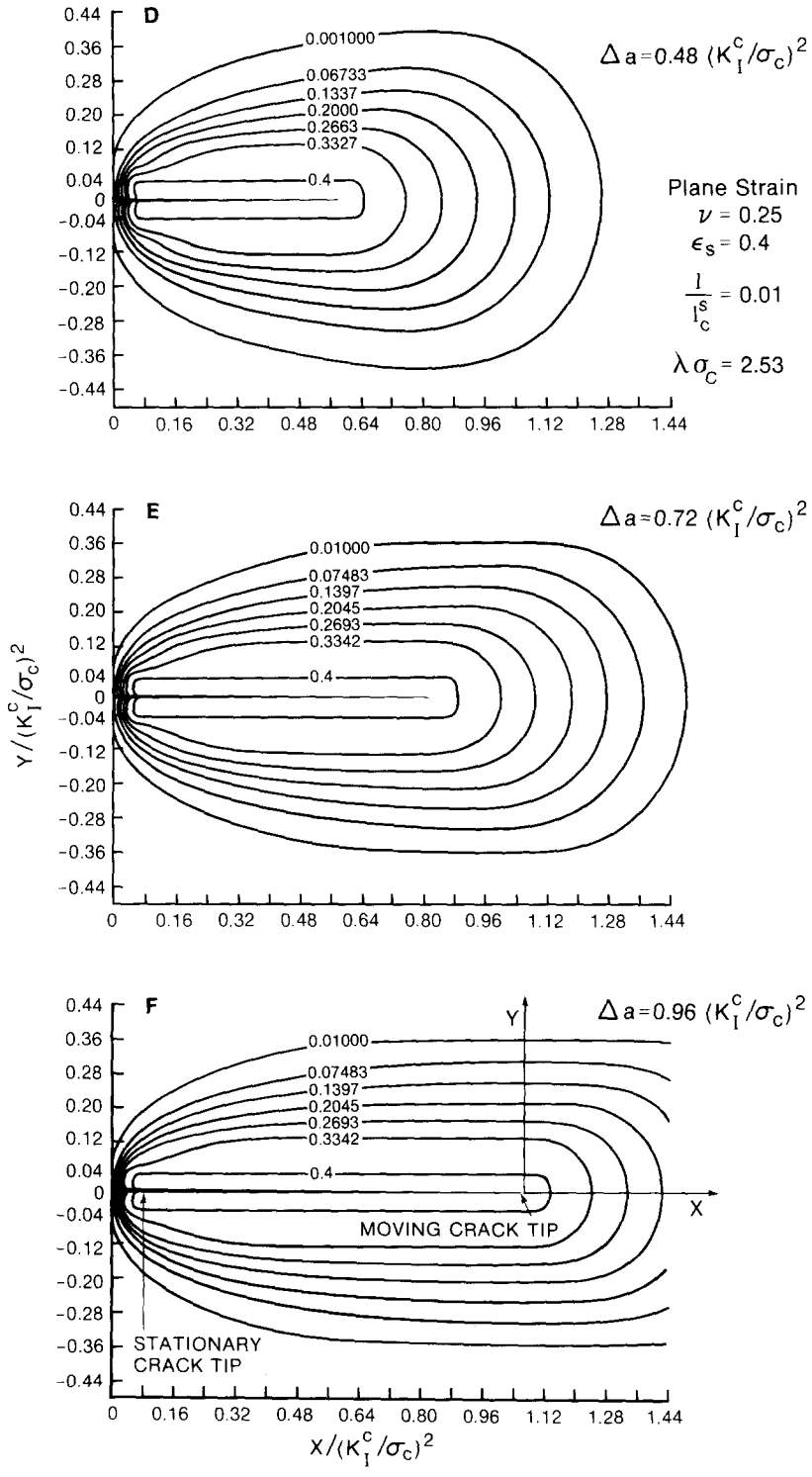


Fig. 5 (continued).

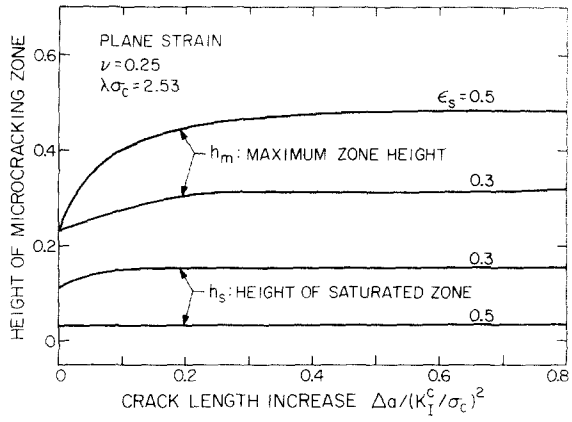


Fig. 6. Height of damage zone versus crack length increase.

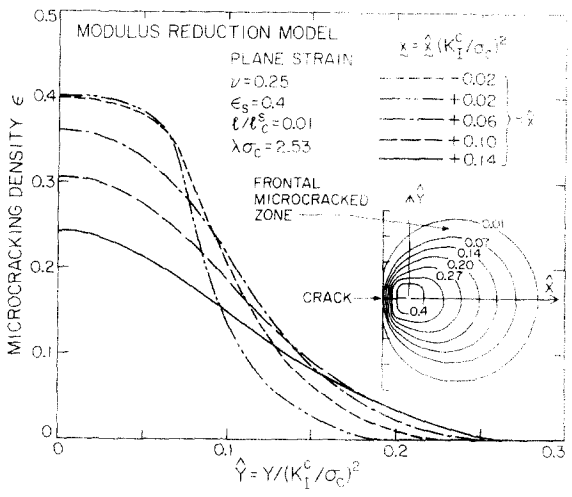


Fig. 8. The microcrack density profile in the y direction at different positions in the frontal microcracked zone.

early in the steady state wake as can be seen in Fig. 7. However, different choices of the dimensionless product $\lambda\sigma_c$ caused slight changes to the microcrack density distribution as reported by Charalambides and McMeeking (1986a). In contrast, the density profiles for the stationary crack were different and nonlinear as can be seen in fig. 8.

Figure 9 shows the R-curves obtained through our finite element crack propagation modeling; i.e. plots of $K_I$ from the applied loads versus $\Delta a$, the crack extension. R-curves for three different saturation values are presented, i.e., $\epsilon_s =$ (0.3, 0.4, 0.5). The actual numerical results are indicated by the point symbols in the figure and smooth curves have been drawn for clarity. The solid symbols correspond to a case when the available energy at the crack tip was either equal to or greater than the critical value $G_c^{tip}$ whereas the

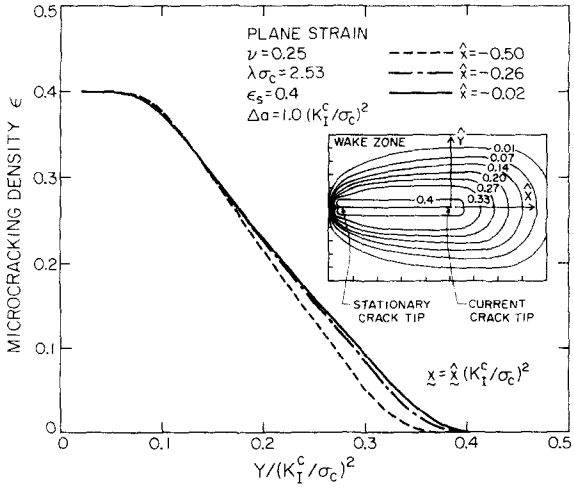


Fig. 7. The microcrack density profile as a function of y at various wake positions.

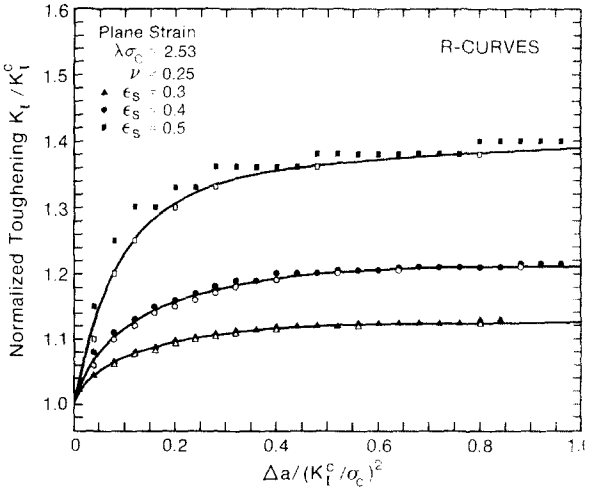


Fig. 9. R-curves obtained through finite element crack propagation simulation.

open symbols indicate that $G^{tip} < G_c^{tip}$ and that the load was then increased. The incremental increase of the applied load resulted in overshooting, which was minimized as much as feasible by taking small load steps.

It should be noted that in Fig. 9 the applied stress intensity factor $K_I$ is normalized by its value $K_I^c$ when crack propagation initiates. The crack tip value of the stress intensity factor has not been used in the plots of R-curves in the figure. It is clear from the previous discussion of the constitutive law and the stationary crack problem that the crack tip stress intensity value for the crack prior to growth is considerably less than the applied value; i.e. for the stationary crack there is shielding of the stress intensification by the microcracks. The result comes about because of the path-independence of $J$ and the reduced modulus value in the near tip saturation zone. From (11) the ratio of the tip value of the stress intensity to the applied value is approximately $\sqrt{1 - \frac{16}{9}\epsilon_s}$ and so for $\epsilon_s = 0.5$, the tip value for the stationary crack is around $\frac{1}{3}$ of the applied value. This result suggests that there could be considerable toughening from this source. However, the weakening effect of microcracks in the near tip region has not been considered in this analysis and, in addition, there is a question as to whether stress intensity factor or energy release rate is the appropriate parameter to use in assessing toughening effects. The point here is that the applied and tip values of the energy release rate are identical for the stationary crack and if this is the critical parameter, no toughening results. (Further details are given by Charalambides and McMeeking (1986a)). In view of these remarks, Fig. 9 has been presented in a manner making no reference to the tip value of the stress intensity factor. Consequently, the R-curve behavior shown in the figure makes reference to the toughness enhancement beyond crack growth initation for the microcracking material, rather than a toughness comparison between the microcracking material and one in which microcracking is suppressed.

The R-curves make it clear that the microcracks shield the crack tip and thus a toughening effect is present. We observe that almost 75% of the toughening occurred during the first three-node

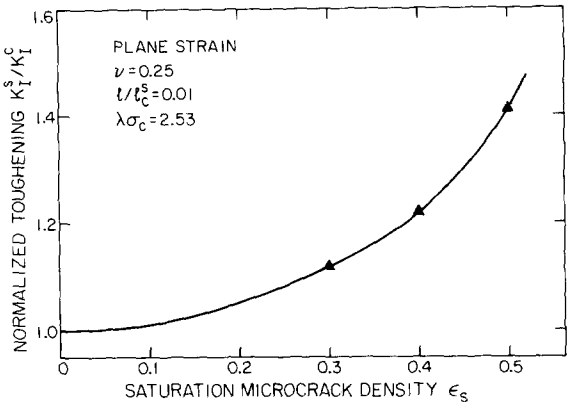


Fig. 10. Trends in toughness with respect to the saturation microcrack density values $\epsilon_s$.

releases, which corresponded to a crack length increase equal to approximately half the height $h_m$ of the initial microcrack zone. According to the same figure, 95% or more of the toughening has occurred by the stage when the crack has advanced by less than twice $h_m$. The trend in toughness with respect to the saturation microcrack density value $\epsilon_s$ is shown in Fig. 10. The steady state asymptote of $K_I$, denoted $K_I^s$, is used as a measure of the toughening on the assumption that instability would occur at $K_I$ levels close to or at that value. We observe a substantial increase of the steady state toughening value as $\epsilon_s \to \frac{9}{16}$ which

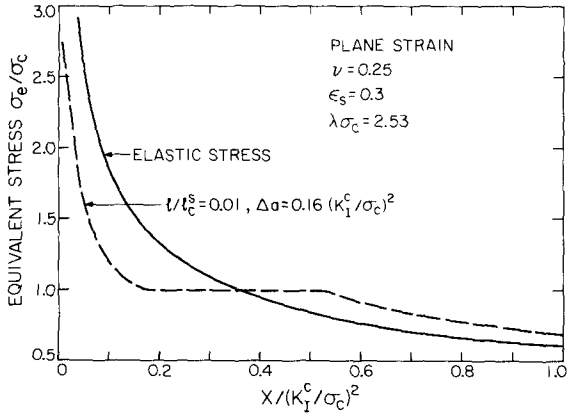


Fig. 11. The equivalent stress $\sigma_e$ ahead of the crack tip during steady state propagation.

is consistent with the approximate results given by Charalambides and McMeeking (1986a).

Figure 11 shows the equivalent stress $\sigma_e$ ahead of the current crack tip after crack extension $\Delta a = 0.16\,(K_I^c/\sigma_c)^2$. Substantial stress reduction was observed in the microcrack region. However, the deviation from the elastic solution diminished to negligible levels at a distance from the crack tip approximately five times the length $x_m$ of the microcrack zone. Due to the reduced modulus, the strains in the inner zone were higher than those of an unmicrocracked material.

## Discussion

### *Relationship to ceramic properties*

As shown by Charalambides and McMeeking (1986a), the parameters of the microcracking law $\lambda$ and $\sigma_c$ in equation (1) can be related to microstructural variables through the theory of Fu (1983) and Evans and Fu (1985a) for microcracking of single phase ceramics. The grain size of the material is $l$ and after cooling to ambient temperature the maximum stress on a grain boundary facet is $\sigma_{max}^R$. This stress is proportional to temperature and depends otherwise on anisotropies of the ceramic (Fu, 1983). There exists also a threshold grain size $l_c^s$ above which the ceramic microcracks spontaneously at ambient temperatures. This critical size depends on the difference between ambient and processing temperatures and also varies from material to material. It can be measured independently. In terms of these quantities

$$\lambda = 9/32\sigma_{max}^R, \tag{13}$$

$$\sigma_c = \sigma_{max}^R\left[\sqrt{l_c^s/l} - 1\right]. \tag{14}$$

The derivation of (13) and (14) is given in more detail by Charalambides and McMeeking (1986a).

These relationships provide two of the three parameters $\lambda$, $\sigma_c$ and $\sigma_m$, needed to characterize the microcracking law. Since $\sigma_m$ is tied up with $\epsilon_s$, the saturation density of microcracks, its value is more difficult to obtain. However, the experimental data (Evans and Langdon, 1976) seems to indicate that at $l/l_c^s = 0.01$ as in our finite element calculations, the amount of toughness increase is about 5%. As can be seen in Fig. 10 where the finite element crack growth results for the toughness ratio $K_I^s/K_I^c$ are plotted against $\epsilon_s$, extrapolation indicates that $\epsilon_s \cong 0.2$ would give satisfactory results. However, those model deductions were based on a more limited model in which the wake of microcracked material was not permitted to widen as the crack grew. The wider zones in the more exact calculation for crack growth clearly contribute more shielding and thus a smaller compliance change is sufficient. It should be noted that the less exact results of Charalambides and McMeeking (1986a) give a trend of toughness against grain size which agrees well with the experimental data. The more exact results for crack growth will also give a similar trend. In the future, more extensive results will be reported for crack growth calculations and those will include the effect of residual strain as well as modulus reduction (Charalambides and McMeeking, 1986b). In those calculations, a wider range of parameter values is being considered and substantial toughening can be expected.

### *Relationship to previous work*

In this paper, as in the work of Charalambides and McMeeking (1986a), the notion of a microcracking continuum solid has been used in finite element calculations to predict microcrack density distributions around the crack tip of a major crack and the effect on the material toughness. However, other approaches, mainly based on discrete microcrack mechanics, have been developed during the recent years. McClintock (1974) and McClintock and Mayson (1977) studied the nucleation, growth and coalescence of microcracks in a two dimensional array of regular hexogonal grains. A statistical failure model was used to predict microcrack nucleation in a biaxial stress field. These microcracks were initially considered stable. However, further load increase caused the microcracks to grow. Finally, at a critical microcrack length, microcrack localization effects led to microcrack coalescence to form macrocracks which limited the applied load to a maximum level. The

microcrack interaction was taken into account by iterative stress analysis. Hoagland, Embury and Green (1975) and Hoagland and Embury (1980) studied the phenomenon of near-tip microcracking using a numerical model of two-dimensional discrete microcracks. These microcracks were placed in the near-tip singular stress field at predestined positions upon satisfaction of a critical normal or shear stress criterion. Approximate microcrack-microcrack and microcrack-macrocrack interactions were taken into account by introducing the singular stress fields associated with each microcrack and enforcing traction free macrocrack surface conditions. R-curve effects were predicted.

Chudnovsky and Kachanov (1983) studied the same problem of small scale microcracking using a double layer potential technique. A closed form solution for the effective stress field for layers of 2-D microcracks in the vicinity of the crack tip was proposed. This solution accounts for the interaction of microcracks among themselves and with the main crack. The traction free microcrack condition was enforced through a lengthy iterative method.

Kachanov (1986) and Kachanov and Montagut (1986) further extended the above analysis. Their method of stress analysis in elastic solids with many cracks was based on a superposition technique with self-consistency to determine the average traction on individual cracks. This method yielded approximate analytical solutions to 2-D as well as 3-D crack arrays of arbitrary geometry. The accuracy was good even when the distance between cracks was smaller than the microcrack length in contrast to the standard self-consistent technique of Budiansky and O'Connell (1975). The shielding effect of a few microcracks near a macrocrack tip was studied. Substantial effects were found. One result of interest is that Kachanov and Montagut (1986) find that microcracks in the wake (i.e. somewhat behind the tip) have little or no effect as far as shielding is concerned. This seems to be in contrast to our results where a wake must be developed before the toughening effect is apparent. However, it must be borne in mind that the shielding implied by the R-curves in Fig. 9 is only part of the overall effect since the crack tip value of stress intensity is not involved in these plots. As discussed previously, there is substantial shielding of the stationary crack tip due to the cluster of microcracks around it. The further increase in shielding due to the generation of a wake as the crack grows is in fact a lesser contribution although more substantial than the results of Kachanov and Montagut (1986) suggest it should be. It can be argued that the results of Kachanov and Montagut (1986) are somehow special although it is not clear why. This can be said for the following reason. If one considers a small circular patch of isotropically microcracked material present in an otherwise intact solid, the shielding effect can be estimated from the work of McMeeking and Evans (1982). Prior to microcracking, the patch is compatible with the surrounding material. After microcracking, the stress in the material around the patch applied to the patch, which now has a lower modulus, will cause it to be larger than the zone in the matrix it occupies. Thus it has effectively dilated and so the result for such dilatant patches as analyzed by McMeeking and Evans (1982) can be used. This shows that at fixed height above the crack, the shielding is maximized when the patch is at an angle $\frac{1}{5}\pi$ from the crack surface. This would place the patch rather far back in the wake. Perhaps the orientations of the cracks and their mutual interactions are important in the results of Kachanov and Montagut (1986) and it should be said that such effects have been omitted completely from the work in this paper and the discussion outlined above. Further investigation of the comparison between the models is warranted.

The interaction of 2-D microcracks with the main crack was also studied by Rose (1986a) using a point source representation for the microcracks and a self-consistent scheme to determine the strength of these sources. A microcrack model consisting of two symmetric microcracks relative to the crack surface was considered. Crack shielding was predicted for favorably oriented microcracks whereas antishielding effects were predicted otherwise.

In all discrete microcrack models mentioned above, the nucleation of microcracks takes place at predestined positions. Under this assumption, the complexity of the calculations reduces to trac-

table levels and useful qualitative information for the phenomenon of microcracking can be obtained as shown by Rose (1986a; 1986b). However, due to the severe microcrack interdependency, the microcrack zone is highly nonuniform and that presents difficulties in predicting new microcrack positions. In that respect, the discrete models are less tractable for computing accurate microcrack densities in the vicinity of the crack tip. In such a case, when detailed analysis of the microcracking phenomenon is needed, a continuum mechanics description is preferred, as suggested by Rose (1986a).

As discussed earlier in this work, the self-consistent formulation of Budiansky and O'Connell (1975) provided the basis for our continuum microcracking model. On the other hand, when a prescribed set of penny shaped microcracks is considered, Margolin's approach (1983; 1984) provides the basis for another continuum mechanics formulation of the microcracking phenomenon. Margolin, using the known stress and displacement fields for a penny shaped crack, constructed statistical relations for the internal stress and displacement fields for the cracked body. When a continuum set of microcracks was assumed, long range interactions were considered by introducing the effective elastic properties of the microcracked solid as in the Budiansky and O'Connell (1975) method. This gave rise to a constitutive law that had the same form of a generalized Maxwell solid. In addition, Margolin's model incorporated relaxation time effects related to the microstructure which makes it suitable for dynamical calculations. However, as described by Chudnovsky (1984), the model of a homogeneous continuum implies that all parameters are averaged over a representative volume and as such, they represent a statistical measure of the material behavior. The description is only valid on length scales that would include many microcracks. In that respect, long range microcrack interactions can be taken into account through the self-consistent formulation of Budiansky and O'Connell which considers a randomly oriented set of microcracks. This formulation is also based on the notion of effective elastic properties for the microcracked material, but the resulting approximate constitutive law is simple and can easily be incorporated in finite element calculations. In addition, microcrack orientation effects and the resulting anisotropy could be considered though Hoenig's (1979; 1982) work, but at the expense of complicating the model. In the continuum model, derived from the above formations, the microcrack density $\epsilon$ is the damage parameter in the sense of Chudnovsky (1984) and Chudnovsky and Moed (1985). Thermodynamic irreversibility is enforced by not allowing $\epsilon$ to decrease, whereas the thermodynamics and kinematics of microcrack nucleation are not considered.

In addition to their discrete micromechanics analysis (1983a, 1985) Horii and Nemat-Nasser (1983b) extended Budiansky and O'Connell's self-consistent formulation to account for load/microcrack induced anisotropies by introducing crack closure effects. In that analysis, they showed that when closed cracks in a compressive stress environment experience frictional sliding, the overall moduli of the microcracked material become anisotropic and dependent on the loading conditions as well as the loading history. As a result the material is characterized by distinct moduli for tension and compression, the latter being load and loading history dependent. Ideally, this should be combined with the work of Hoenig (1979; 1982) for the elastic response of materials with an anistropic distribution of microcracks. Indeed, the framework for this is already there in the work of Horii and Nemat-Nasser (1983b). As discussed previously, the effect of the large facet residual stresses in the alumina ceramic produces a response which is substantially isotropic and, except for large compressions, symmetric about zero stress after microcracking has occurred. Undoubtedly, the anistropies involved in the work of Horii and Nemat-Nasser (1983b) and Hoenig (1979, 1982) should be included in an appropriate way, to enhance the model of microcracking for alumina. Perhaps this will be done in future developments of this work.

In recent work, Hutchinson (1986) has provided an alternate continuum mechanics treatment of modulus reduction toughening due to microcracking. Residual strain effects have also been included in this work. A perturbation method

is used to obtain the shielding effect of the modulus reduction and so must be restricted to relatively small compliance changes. However, this would include the case of $\epsilon_s = 0.1$ that we have found to be relevant for alumina. There are differences in detail due to choice of microcracking criterion and rate, but the results of Hutchinson (1986) are substantially in agreement with our own.

The previous paragraphs summarize the treatments of the micromechanics in the various discrete microcrack models mentioned above. Almost all models were based on two assumptions which reduced the complexities to tractable levels. The microcracks were chosen to be two dimensional and they were assumed to nucleate at prechosen positions. Even under these assumptions the most advanced models of Chudnovsky and Kachanov (1983), Kachanov (1986), Kachanov and Montagut (1986) and Rose (1986a) require very extensive calculations when a large set of microcracks is used. Except for Margolin's (1983) method and Kachanov's (1986), additional development would be required for the above models before they could be used in three dimensional problems. On the other hand, a continuum mechanics description of the microcracking phenomenon like ours, Margolin's (1983), and that of Hutchinson (1986) provides an effective technique for computing reasonably accurate microcrack densities. As a consequence, macroscopic effects, for example toughening, can be studied in relation to the microstructure. Finite microcracks can be assumed and microcrack induced anisotropies as well as residual strain effects can readily be incorporated into the model. In addition, three dimensional finite element calculations can be carried out without substantially increasing the complexity of the problem. It is likely that the progress in the area of microcracking of brittle materials will depend on a combination of discrete and continuum methods.

## Closure

The modulus reduction continuum mechanics model proposed in earlier work (Evans and Fu, 1985b; Evans and Faber, 1984; Charalambides and McMeeking, 1986a) contains the necessary non-linear features that give rise to an R-curve during crack propagation. The microcrack zone widens initially during crack growth, but later the wake of microcracked material becomes parallel to the crack surface and steady state conditions prevail with a flat asymptote for the R-curve. The R-curves are initially relatively steep. The results indicate that the toughness of materials would be favorably affected by near tip microcracking as long as damaging effects caused by the weak nature of the microcracked material are not overwhelming. Further understanding of this point, the incorporation of residual strain effects, plus more extensive calculations are required for progress on the phenomenon of near tip microcracking.

## Appendix. Strain energy density calculations

The microcracking law given by (1) and the constitutive law of (3) allow us to determine the strain energy density for a microcracking material. Let $W$ be the strain energy density, then

$$W = \int_{\epsilon_{ij}} \sigma_{kl}\, \mathrm{d}\epsilon_{kl} \tag{i}$$

and

$$\mathrm{d}\epsilon_{kl} = \frac{f+\nu}{E}\, \mathrm{d}\sigma_{kl} - \frac{\nu}{E}\, \mathrm{d}\sigma_{jj}\delta_{kl} + \frac{\mathrm{d}f}{E}\epsilon_{kl}. \tag{ii}$$

Recall that $f$ is a piecewise continuous function of $\sigma$, i.e.,

$$f = \begin{cases} 1.0 \quad \text{if } (\sigma_{ij}\sigma_{ij})^{1/2} < \sigma_c, \\ \dfrac{1}{1 - \frac{16}{9}\lambda\left((\sigma_{ij}\sigma_{ij}^{1/2}) - \sigma_c\right)} \\ \quad \text{if } \sigma_c \leqslant (\sigma_{ij}\sigma_{ij})^{1/2} \leqslant \sigma_m, \\ \dfrac{1}{1 - \frac{16}{9}\lambda(\sigma_m - \sigma_c)} \quad \text{if } (\sigma_{ij}\sigma_{ij})^{1/2} \geqslant \sigma_m. \end{cases} \tag{iii}$$

The strain energy can now be expressed as a continuous function of $f$ which, in itself, is stress dependent through (iii). By carrying out the in-

tegration in (i), we find the strain energy density to be

$$W = (1/2E)\Big[(1+\nu)\sigma_c^2 + (f+\nu)\big(\sigma_c + (9/16\lambda)(1-1/f)\big)^2 - \nu\sigma_{kk}^2 + 2\phi(f, \nu, \lambda, \sigma_c)\Big] \qquad \text{(iv)}$$

where

$$\phi(x, \nu, \lambda, \sigma_c) = (9/16\lambda)^2\Big[\big(1+\tfrac{16}{9}\lambda\sigma_c\big)^2 x - \big(1+\tfrac{16}{9}\lambda\sigma_c\big)\ln x - \big(1+\tfrac{16}{9}\lambda\sigma_c\big)\nu/x + \tfrac{1}{2}\nu/x - \big(1+\tfrac{16}{9}\lambda\sigma_c\big)^2 + \nu\big(1+\tfrac{16}{9}\lambda\sigma_c\big) - \tfrac{1}{2}\nu\Big]. \qquad \text{(v)}$$

Notice that (iv) for the strain energy is good for both loading and unloading cases, providing that the internal microcracking variable $f$ used is the maximum previously experienced by the particular material point and the stresses correspond to the current stress state.

## Acknowledgement

The authors would like to express their appreciation to Dr. Anthony G. Evans for his insightful comments made throughout this work. We would like to acknowledge also that this research was supported by the Office of Naval Research through contract N000014-85-K-0883 with the University of California, Santa Barbara.

## References

Budiansky, B. and R.J. O'Connell, (1975), "Elastic moduli of a cracked solid", *Int. J. Solids Struct. 12*, 81.

Charalambides, P.G. (1986), "Near tip mechanics of stress induced microcracking in brittle materials", PhD Dissertation, University of Illinois at Urbana-Champaign.

Charalambides, P.G. and R.M. McMeeking (1986a), "Near tip mechanics of stress induced microcracking in brittle materials", to be published.

Charalambides, P.G. and R.M. McMeeking (1986b). "Toughening due to stress induced microcracking with residual strains", to be published.

Chudnovsky, A. (1984), "Statistics of thermodynamics of fracture", *Int. J. Engng. Sci. 22*, 989.

Chudnovsky, A. and M. Kachanov (1983), "Interaction of a crack with a field of microcracks", *Lett. Appl. Engng. Sci. 21*, 1009.

Chudnovsky, A. and A. Moed (1985), "Thermodynamics of translation crack layer propagation", *J. Mat. Sci. 20*, 630.

Evans, A.G. (1974), "The role of inclusions in the fracture of ceramic materials", *J. Mater. Sci. 9*, 1145.

Evans, A.G. and K.T. Faber (1981), "Toughening of ceramics by circumferential microcracking", *J. Amer. Ceram. Soc. 64*, 394.

Evans, A.G. and K.T. Faber (1984), "Crack-growth resistance of microcracking brittle materials", *J. Amer. Ceram. Soc. 67*, 255.

Evans, A.G. and Y. Fu (1985a), "Some effects of microcracks on the mechanical properties of brittle solids—I. Stress strain relations", *Acta Metall. 33*, 1515.

Evans, A.G. and Y. Fu (1985b), "Some effects of microcracks on the mechanical properties of brittle solids—II. Microcrack toughening', *Acta Metall. 33*, 1525.

Evans, A.G., A.H. Heuer and D.L. Porter (1977), "The fracture toughness of ceramics", in: D.M.R. Taplin, ed., *Fracture 1977, Vol. 1*, Pergamon Oxford, 529.

Evans, A.G. and T.G. Langdon (1976), "Structural ceramics", *Prog. in Mater. Sci. 21*, 171.

Friedman, M., J. Handin and G. Alani (1972), "Fracture-surface energy of rocks", *Int. J. Rock Mech. Min. Sci. 9*, 757.

Fu, Y. (1983), "Mechanics of microcracking toughening in ceramics", Ph.D. Dissertation, University of California, Berkeley.

Hoagland, R.G. and J.D. Embury (1980), "A treatment of inelastic deformation around a crack tip due to microcracking", *J. Amer. Ceram. Soc. 63*, 404.

Hoagland, R.G., J.D. Embury and D.J. Green (1975), "On the density of microcracks formed during the fracture of ceramics", *Scrip. Metall. 9*, 907.

Hoagland, R.G., C.W. Marshall, A.R. Rosenfield, G. Hollenberg and R. Ruh (1974), "Microstructural factors influencing fracture toughness of hafnium titane", *Mater. Sci. and Engng. 15*, 51.

Hoenig, A. (1979), "Elastic moduli of a non-randomly cracked body", *Int. J. Solids Struct. 15*, 137.

Hoenig, A. (1982), "Near-tip behavior of a crack in a plane anistropic elastic body", *Engng. Fracture Mech. 16*, 393.

Horii, H. and S. Nemat-Nasser (1983a), "Estimates of stress intensity factors for interacting cracks", in: U. Yuceoglu et al., eds., *Advances in Aerospace Structures, Materials and Dynamics*, ASME, New York, 111.

Horii, H. and S. Nemat-Nasser (1983b), "Overall moduli of solids with microcracks: Load-induced anisotropy", *J. Mech. Phys. Solids 31*, 155.

Horii, H. and S. Nemat-Nasser (1985), "Elastic fields of interacting inhomogeneities", *Int. J. Solids Struct 21*, 731.

Hubner, H. and W. Jillek (1977), "Sub-critical crack extension and crack resistance in polycrystalline alumina", *J. Mater. Sci. 12*, 117.

Hutchinson, J.W. (1986), "Crack-tip shielding by micro-cracking in brittle solids", to be published.

Kachanov, M. (1986), "Interaction of a crack with certain microcrack arrays", *Engng. Fracture Mech.*, to appear.

Kachanov, M. and E. Montagut (1986), "Elastic solids with many cracks: A simple method of analysis", *Int. J. Solids Struct.*, to appear.

Knehans, R. and R. Steinbrech (1982), "Memory effects of crack resistance during slow crack growth in notched $Al_2O_3$ bend specimens", *J. Mater. Sci. Lett. 1*, 327.

Margolin, L.G. (1983), "Elastic moduli of a cracked body", *Int. J. Fracture 22*, 65.

Margolin, L.G. (1984), "Microphysical models for inelastic material response", *Int. J. Engng. Sci. 22*, 1171.

Marshall, D.M. (1986), Presentation at the Winter Study Group, University of California, Santa Barbara.

McClintock, F.A. (1974), "Statistics of brittle fracture", in: R.C. Bradt et al., eds., *Fracture Mechanics of Ceramics, Vol. 1*, Plenum, New York, 93.

McClintock, F.A. and H.J. Mayson (1977), "Principal stress effects on brittle crack statistics", Technical Report RADC-TR-77-368, Center of Materials Science and Technology, MIT, Cambridge, 113.

McMeeking, R.M. and A.G. Evans (1982), "Mechanics of transformation toughening in brittle materials", *J. Amer. Ceram. Soc. 65*, 242.

Parks, D.M. (1974), "A stiffness derivative finite element technique for determination of elastic crack tip stress intensity factors", *Int. J. Fracture 10*, 487.

Parks, D.M. (1978), "The virtual crack extension method for nonlinear material behavior", in: A.R. Luxmoore and D.R.J. Owen, eds., *Numerical Methods in Fracture Mechanics*, 464.

Rice, J.R. (1968), "Mathematical analysis in the mechanics of fracture", in H. Liebowitz, ed., *Fracture: An Advanced Treatise, Vol. 2*, Academic Press, New York, 192.

Rose, L.R.F. (1986a), "Microcrack interaction with a main crack" to be published.

Rose, L.R.F. (1986b), "Effective fracture toughness of microcracked materials", *J. Amer. Ceram. Soc. 69*, 212.